# Model-based Reconstruction of Distributed Phenomena using Discretized Representations of Partial Differential Equations

Felix Sawo, Kathrin Roberts and Uwe D. Hanebeck

Intelligent Sensor-Actuator-Systems Laboratory
Institute of Computer Science and Engineering
Universität Karlsruhe (TH)
Karlsruhe, Germany
{sawo,roberts}@ira.uka.de, uwe.hanebeck@ieee.org

**Abstract.** This article addresses the model-based reconstruction and prediction of distributed phenomena characterized by partial differential equations, which are monitored by sensor networks. The novelty of the proposed reconstruction method is the systematic approach and the integrated treatment of uncertainties, which occur in the physical model and arise naturally from noisy measurements. By this means it is possible not only to reconstruct the entire phenomenon, even at non-measurement points, but also to reconstruct the complete density function of the state characterizing the distributed phenomenon. In the first step, the partial differential equation, i.e., *distributed*-parameter system, is spatially and temporally decomposed leading to a *finite*-dimensional state space form. In the next step, the state of the resulting *lumped*-parameter system, which provides an approximation of the solution of the underlying partial differential equation, is dynamically estimated under consideration of uncertainties. By using the estimation results, several additional tasks can be achieved by the sensor network, e.g. optimal sensor placement, optimal scheduling, model improvement, and system identification. The performance of the proposed model-based reconstruction method is demonstrated by means of simulations.

**Keywords.** Stochastic systems, Baysian estimation, model-based reconstruction, distributed phenomenon, environmental monitoring, sensor-actuator-network.

## 1 Introduction

Recent developments in wireless sensor network technology and miniaturization of sensor nodes make it possible to exploit sensor networks [14] [18] for monitoring the natural environment [22] [4]. Such sensor networks can be used in industrial, medical, urban, and many other environments. Furthermore, applying sensor networks can provide new data for environmental science, such as climate models, as well as growth and reproduction of coral reefs indicated by physical environmental factors, e.g. temperature, water movement, salt concentration, and pollutant concentration. Additional examples are reconstruction of fluid-flow in a thermal reactor [6], and reconstruction of the surface motion of a beating heart in minimally invasive surgery [16].

In practical implementations the sensor nodes are normally densely deployed either inside the phenomenon or very close to it. For such scenarios the number of sensor nodes should be as low as possible because of economical and energy reasons; the same holds for the measurement rates. In general, it can be stated the lower the measurement rate of the sensor nodes the higher their durability. Thus, a trade-off between energy costs and accuracy has to be found. In order to get meaningful and accurate information not only at the sensor nodes itself but also between these nodes, the *model-based* reconstruction of the distributed phenomenon is of major significance. By the consideration of additional background information in form of a physical model, the approach proposed in this chapter achieves accurate reconstruction results even for a low number of sensor nodes and even between the individual sensor nodes.

In general, physical phenomena can be classified into *distributed*-parameter systems and *lumped*-parameter systems. The key characteristic of a lumped-parameter system is that the state, which uniquely describes the system behavior, depends only on time, e.g. bird swarms or swarms of robots. Such systems can be conveniently described by a set of *ordinary* differential equations. On the other hand, the key characteristic of distributed-parameter systems is that the state not only depends on time but also on the location, e.g. irrotational fluid flow, heat conduction, and wave propagation [13] [19]. The behavior of distributed-parameter systems can be described by a set of *partial* differential equations.

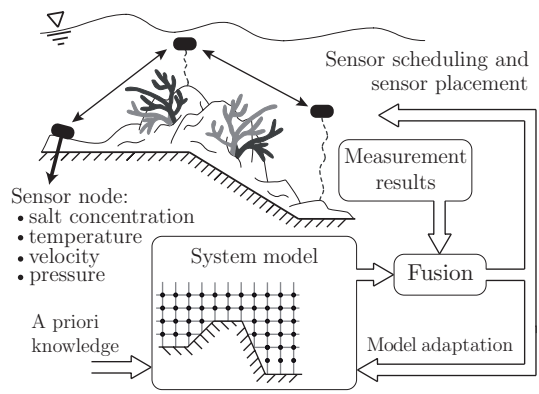


**Fig. 1** Visionary scenario for the reconstruction and the observation of a distributed phenomenon by means of a sensor network: observation of a coral reef.

For the prediction of the state characterizing uniquely the distributed phenomenon we present a novel systematic approach, which allows the integrated treatment of uncertainties both occuring in the physical model and arising from noisy measurements. Basically, data from the sensor network in form of measurements as well as data from a physical model are used to derive the best possible estimate for the state of a distributed phenomenon; even at non-measurement points. The estimation results on the other hand can be used for finding the optimal placement and measurement time sequences for the sensor nodes similar to [3], and furthermore can be used for improving the parameter values of the used physical model, or for system identification to name just a few applications, (see Fig. 1).

Usually, a model-based reconstruction approach based on a distributed-parameter system description is quite complicated. The reason is for a Bayesian estimation method usually a lumped-parameter system description is used. To cope with this problem, the system description has to be converted from a distributed-parameter description to a lumped-parameter description. This means the partial differential equations characterizing the distributed phenomena has to be solved. Such equations can be solved for example by the finite-element method or the finite-difference method [2]. The unstructured nature of those methods allows a detailed geometrical description of complex geometries. Additionally, it is possible to solve even nonlinear partial differential equations. However, many parameters describing uniquely the state of the distributed phenomenon are necessary to achieve appropriate convergence.

On the other hand, there are modal analysis methods using a set of *global* expansion functions. These methods just need a few parameters for characterizing a smooth solution of the partial differential equation [19]. The drawback, however, is that for modal analysis global expansion functions can be found only for problems with simple boundary conditions.

Combining these two general approaches, leads to the so-called finite-spectral method [5] [7] [11] [12] [15]. Basically, this method approximates the solution within each element with a set of orthogonal polynomials, such as Legendre polynomials, or Chebyshev polynomials. Thus, it combines the geometrical flexibility of conventional finite-element methods with the exponential convergence rates associated with the modal analysis.

The novelty of this research work is the model-based observation of distributed phenomena by a sensor network under consideration of uncertainties both occuring in the physical model, i.e., system model, and arising from noisy measurements. Here, we extend and generalize our previous research work [19] in such a way that both the system model and the measurement model are derived by the finite-spectral method. Using this method, it turns out that even nonlinear phenomena with complex boundary conditions can be reconstructed and predicted in a systematic manner.

The remainder of this chapter is organized as follows. In Sect. 2, a rigorous formulation of the problem of the reconstruction of distributed phenomena characterized by partial differential equations is given. In Sects. 3 and 4, a spatial and temporal decomposition of the partial differential equation is performed. This allows the approximation of the partial differential equation (distributed-parameter system) by means of a finite-dimensional system in state space form (lumped-parameter system). Finally, in Sect. 5 the centralized estimator is derived and its performance is demonstrated by means of simulations: As an example, the temperature distribution in a heat conductor is reconstructed by means of a sensor network. The results presented in this chapter were prepublished in the *Proceedings of the 3rd International Conference on Informatics in Control, Automation and Robotics*, [20]. However explanations of the proposed model-based reconstruction method are presented in a considerably extended form in this chapter.

## 2 Problem Formulation

The main goal is to design a dynamic system model for the purpose of estimating the state of a distributed phenomenon monitored by a sensor network. A large number of distributed phenomena, such as irrotational fluid flow, heat conduction, and wave propagation [19], can be described by means of a set of linear partial differential equations.

In this article, for simplicity and brevity only a one-dimensional linear partial differential equation is used, although similar expressions can be found for the multi-dimensional nonlinear case. The one-dimensional linear partial differential equation is given by

$$\mathbb{L}(f) = \frac{\partial f(z,t)}{\partial t} - c\,\frac{\partial^2 f(z,t)}{\partial z^2} - s(z,t) = 0 \ , \tag{1}$$

where $f(z,t)$ denotes the solution of the partial differential equation, e.g. temperature at a certain location $z$ and at a certain time $t$, $s(z,t)$ represents the source term, and $c$ is a positive constant. Considering the solution in a domain $\Omega = \{z \,|\, 0 \leq z \leq L\}$, we assume following boundary conditions

$$f(z = L, t) = g_D \ , \qquad \frac{\partial f(z = 0, t)}{\partial z} = g_N \ , \tag{2}$$

where $g_D$ is referred to as a *Dirichlet* boundary condition and $g_N$, specifying a condition on the derivative, is the so-called *Neumann* boundary condition.

The aforementioned partial differential equation (1) describes the distributed phenomenon in an *infinite*-dimensional state space. However, in order to estimate and reconstruct the state of a distributed phenomenon by means of a Bayesian estimation approach, the partial differential equation has to be characterized by a *finite*-dimensional state space form. Thus, the partial differential equation (distributed-parameter system) has to be approximated by means of a finite-dimensional system in state space form, according to

$$\underline{x}_{k+1} = \mathbf{A}_k\,\underline{x}_k + \mathbf{B}_k\,\underline{u}_k + \underline{w}_k \ , \tag{3}$$

where $\underline{x}_k$ contains the individual states characterizing the time evolution of the distributed phenomenon and the matrix $\mathbf{A}_k$ maps the current state vector at time step $k$ to the next state vector at time step $k+1$. The noise vector $\underline{w}_k$ contains both driving input $\Delta\underline{u}_k$ noises and subsumed endogenous uncertainties $\underline{d}_k$, e.g. modeling errors, according to

$$\underline{w}_k = \begin{bmatrix}\mathbf{I}\ \mathbf{I}\end{bmatrix} \begin{bmatrix}\mathbf{B}\Delta\underline{u}_k \\ \underline{d}_k\end{bmatrix} \ , \tag{4}$$

where $\mathbf{I}$ is the identity matrix. At this point it is worthwhile to mention that linear partial differential equations can always be approximated by a linear system model according to (3). However, the approximation of nonlinear partial differential equations leads to a nonlinear system model.

Furthermore, it is assumed that the measurements $\hat{\underline{y}}_k$ are related linearly to the state vector $\underline{x}_k$, according to

$$\hat{\underline{y}}_k = \mathbf{H}_k\,\underline{x}_k + \underline{v}_k \ , \tag{5}$$

where $\mathbf{H}_k$ denotes the measurement gain matrix and $\underline{v}_k$ represents the measurement uncertainties.

Once the system equation and the measurement equation are derived, the state vector $\underline{x}_k$ characterizing the distributed phenomenon can be estimated by means of the Kalman filter for the linear case [1], or nonlinear estimation procedures [9] for the nonlinear case.

## 3 Spatial Decomposition (ODE-System)

In this section, we present the spatial decomposition allowing the conversion of the partial differential equation (1) into a set of ordinary differential equations (ODE-System). It is well-known that the finite-difference, the finite-element, and the finite-spectral method may be used with the same numerical methodology described in the next section, namely the *Galerkin* formulation [2] [11].

### 3.1 Galerkin Formulation

The first basic ingredient for the conversion of the partial differential equation into a set of ordinary differential equations is the decomposition of the solution domain $\Omega = \{z \,|\, 0 \leq z \leq L\}$ into $N_{el}$ subdomains $\Omega^e$, which are the so-called *finite elements*. These subdomains are defined by the element boundary-nodes, $z_i$, for $i = 0, 1, \ldots, N_{dof} - 1$, where $z_0 = 0$ and $z_{N_{dof}-1} = L$. The elemental decomposition of the solution domain $\Omega$ into several subdomains $\Omega^e$ is visualized by means of an example in Fig. 2a.

For the second basic ingredient, it is assumed that the solution $f(z,t)$ in the solution domain $\Omega$ can be represented by a piecewise approximation $\tilde{f}(z,t)$ according to

$$\tilde{f}(z,t) = \sum_{i=0}^{N_{dof}-1} \Psi_i(z)\, \alpha_i(t) \quad , \tag{6}$$

where $\Psi_i(z)$ are analytic functions called the *shape functions*, e.g. see Fig. 2b, and $N_{dof}$ denotes the aforementioned degree of freedom of the resulting system description.

It is important to note that the individual shape functions $\Psi_i(z)$ are defined in the entire solution domain $\Omega$. Furthermore, because of numerical advantages the shape functions $\Psi_i$ should be constructed in such way that the so-called *cardinal interpolation property* is satisfied

$$\Psi_i(z_j) = \delta_{ij} \quad , \tag{7}$$

where $z_j$ represents the element end-nodes and $\delta_{ij}$ is Kronecker's delta,

$$\delta_{ij} = \begin{cases} 1 \; i = j \\ 0 \; i \neq j \end{cases} \tag{8}$$

In other words, the $i$th shape function $\Psi_i$ takes the value of unity at the $i$th node, and remains zero at the other nodes. This essential property of the shape function can be easily recognized in Fig. 2b. Furthermore, because of the cardinal interpolation property, the

coefficients $\alpha_i(t)$ have a physical interpretation in that they represent the approximated solution $\tilde{f}(z_j, t)$ at the element end-nodes $z_j$.

The essence of all spatial decomposition methods such as the finite-difference, the finite-element, and the finite-spectral method lies in the choice of the shape functions $\Psi_i(z)$. This function is to be specified in more detail later.

Due to the fact that the approximated solution $\tilde{f}(z,t)$ cannot satisfy the partial differential equation (1) everywhere in the region of interest, a *residual* $R_\Omega$ according to

$$\mathbb{L}\left(\tilde{f}(z,t)\right) = R_\Omega\left(\tilde{f}(z,t)\right) \neq 0 \tag{9}$$

remains. A common method known as the *Galerkin* formulation is based on finding a way to make this residual small in some sense; achieved by minimizing an appropriate number of *weighted integrals*. The most popular choice for the weighting functions is the *shape function* itself leading to following weighted integrals

$$\int_\Omega \Psi_i(z)\mathbb{L}\left(f(z,t)\right) dz = 0 \ , \tag{10}$$

with $i = 0, 1, \ldots, N_{dof} - 1$. Replacing both the solution function $f(z,t)$ and the input function $s(z,t)$ by the finite expansion (6), denoted by $\tilde{f}(z,t)$ and $\tilde{s}(z,t)$, respectively, leads to following weighted integrals over the solution domain $\Omega$

$$\int_\Omega \Psi_i(z)\left[\frac{\partial \tilde{f}(z,t)}{\partial t} - c\,\frac{\partial^2 \tilde{f}(z,t)}{\partial z^2} - \tilde{s}(z,t)\right] dz = 0 \tag{11}$$

with $i = 0, 1, \ldots, N_{dof} - 1$. It can be stated that the minimization of this integral automatically leads to the best numerical approximation of the solution $f(z,t)$ of the partial differential equation [2].

Expression (11) can now be reformulated by using the rules of product differentiation, according to

$$\begin{aligned}\int_\Omega \Psi_i(z)\frac{\partial \tilde{f}(z,t)}{\partial t} dz &= \int_\Omega \Psi_i(z)\tilde{s}(z,t)dz + \\ c\int_\Omega \left[\frac{\partial}{\partial z}\left(\Psi_i(z)\frac{\partial \tilde{f}(z,t)}{\partial z}\right) - \frac{d\Psi_i(z)}{dz}\frac{\partial \tilde{f}(z,t)}{\partial z}\right] dz\end{aligned} \tag{12}$$

Applying the fundamental theorem of calculus for the evaluation of the last term on the right-hand side leads to

$$\begin{aligned}\int_\Omega \Psi_i(z)\frac{\partial \tilde{f}(z,t)}{\partial t} dz &= \int_\Omega \Psi_i(z)\tilde{s}(z,t)dz \\ - c\int_\Omega \frac{d\Psi_i(z)}{dz}\frac{\partial \tilde{f}(z,t)}{\partial z}dz &+ c\left[\Psi_i(z)\frac{\partial \tilde{f}(z,t)}{\partial z}\right]_{\partial\Omega_l}^{\partial\Omega_r}\end{aligned} \tag{13}$$

where the last term on the right-hand side contains the boundary conditions, i.e., $\partial\Omega_r$ and $\partial\Omega_l$ denote the right-hand and left-hand boundary, respectively. This weighted

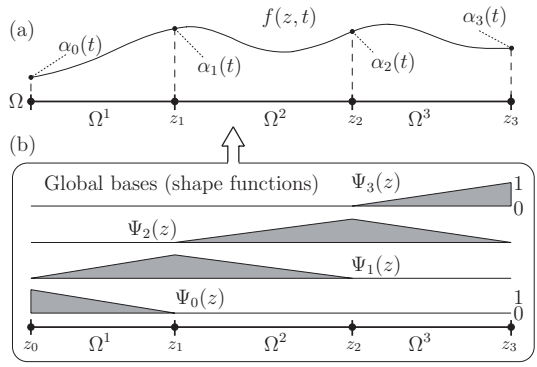


**Fig. 2** The solution $f(z,t)$ of the partial differential equation is approximated by $\tilde{f}(z,t)$ depending on the shape functions $\Psi_j(z)$ and their weighting coefficients $\alpha_j$(t). **(a)** Elemental decomposition of the solution domain $\Omega$ into several subdomains $\Omega^e$. **(b)** Shape functions $\Psi_i(z)$ for the linear case.

residual statement is known as the *weak formulation* of the partial differential equation (1).

As it is shown in the next sections, by specifying the shape functions $\Psi_i(z)$ the weighted residual statement (13) can be reduced to a system of ordinary differential equations in terms of $\alpha_i(t)$, i.e., the semi-discrete version of problem (1),

$$\mathbf{M}_G\, \underline{\dot{x}}(t) = \mathbf{M}_G\, \underline{u}(t) - c\, \mathbf{D}_G\, \underline{x}(t) + \underline{b}^*(t) \tag{14}$$

In this system, $\mathbf{M}_G$ is called the global *mass* matrix and $\mathbf{D}_G$ is the global *diffusion* matrix, and $\underline{b}^*$ represents the boundary conditions. The vector $\underline{x}(t)$ and $\underline{\dot{x}}(t)$ are the state vectors of the unknown weighting coefficients $\alpha_i(z)$ and their derivatives

$$\underline{x}(t) = \left[\alpha_0(t), \alpha_1(t), \cdots, \alpha_{N_{dof}-1}(t)\right]^T \tag{15}$$

It is important to note that the entries of the matrices $\mathbf{M}_G$ and $\mathbf{D}_G$, and the state vector $\underline{x}(t)$ merely depend upon the choice of the shape functions $\Psi_i(z)$, as shown in the following sections.

The next sections are devoted to appropriate definitions of the shape functions $\Psi_i(z)$. First, the $h$-type expansion functions decomposing the solution domain into small subdomains are considered; $\Psi_i(z)$ are usually linear functions or simple polynomials. Then, based on this decomposition, it is possible to introduce additional supporting nodes within the subdomains; the so-called nodal $p$-type expansion functions using higher-order orthogonal polynomials. Finally, the shape functions $\Psi_i(z)$ can be defined by a set of orthogonal polynomials of different order or modes, called modal $p$-type expansion functions. For each type it is shown that the global mass matrix $\mathbf{M}_G$ and the global diffusion matrix $\mathbf{D}_G$ can be calculated in a similar manner.

### 3.2 Elemental Decomposition ($h$-type extension)

In this section, the decomposition of the solution domain $\Omega$ into smaller subdomains $\Omega^e$ is demonstrated in more detail. This process, which is referred to as the *h-type extension*,

basically reduces the sizes of the individual subdomains $\Omega^e$ in order to achieve convergence of the approximated solution.

Here, the decomposition process is explained and visualized by means of simple polynomials for the shape functions $\Psi_i(z)$. However, the same techniques can be exploited with higher-order polynomial expressions, as shown in the next sections. The decomposition of the solution domain into subdomains and the respective shape functions for linear polynomials are visualized in Fig. 2.

Substituting the finite expansion (6) into the weak formulation (13) of the partial differential equation yields the following individual terms of the weak formulation

$$\int_\Omega \Psi_i(z) \frac{\partial \tilde{f}(z,t)}{\partial t} dz = \sum_{j=0}^{N_{dof}-1} M_{ij}^g \frac{d\alpha_j(t)}{dt} \tag{16}$$

$$\int_\Omega \frac{d\Psi_i(z)}{dz} \frac{\partial \tilde{f}(z,t)}{\partial z} dz = \sum_{j=0}^{N_{dof}-1} D_{ij}^g \alpha_j(t) \tag{17}$$

$$\int_\Omega \Psi_i(z) \tilde{s}(z,t) dz = \sum_{j=0}^{N_{dof}-1} M_{ij}^g \hat{s}_j(t) \tag{18}$$

The individual entries $M_{ij}^g$ and $D_{ij}^g$, defined by

$$\begin{aligned} M_{ij}^g &= \int_\Omega \Psi_i(z) \Psi_j(z) dz \ , \\ D_{ij}^g &= \int_\Omega \frac{d\Psi_i(z)}{dz} \frac{d\Psi_j(z)}{dz} dz \ , \end{aligned} \tag{19}$$

can be assembled to the global mass matrix $\mathbf{M}_G$ and the global diffusion matrix $\mathbf{D}_G$, respectively. At this point it can be easily recognized that this always leads to the ordinary differential equation given in (14).

Furthermore, it is noted that in the case of piecewise affine shape functions $\Psi_i(z)$ this leads to the finite-difference formula, which can be regarded as a special case of the finite-element method [2].

### 3.3 Nodal Polynomial Expansion

This section describes how the weak formulation (13) is decomposed in space using higher order polynomials; also called *p-type expansion*. Assuming a fixed mesh, these methods achieve a higher accuracy of the solution by increasing the polynomial order *inside* the element.

Since a consideration of the expansion in terms of global modes $\Psi_i(z)$ is uneconomical and numerically intractable, especially when using a large number of elements, it is reasonable to introduce a standard element $\Omega_{st}$, such that

$$\Omega_{st} = \{\xi \mid -1 \leq \xi \leq 1\} \ . \tag{20}$$

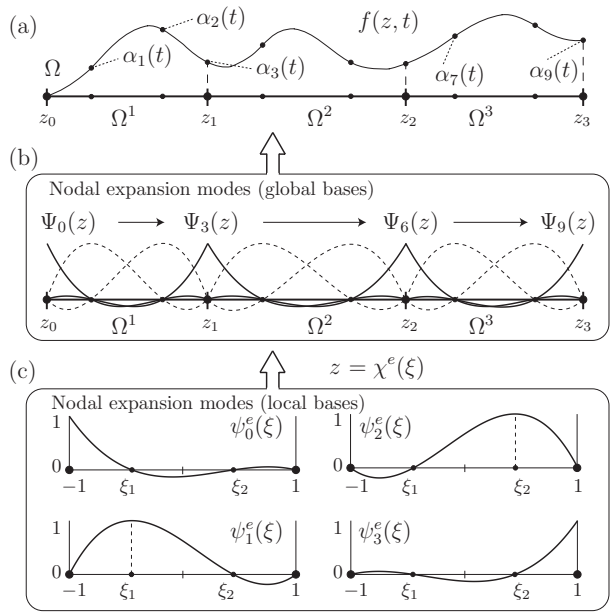


**Fig. 3** Approximation of the solution $f(z,t)$ by means of a nodal polynomial expansion, e.g. Legendre polynomials for $m = 4$ refinement. **(a)** Elemental decomposition of the solution domain $\Omega$ into several subdomains $\Omega^e$. **(b)** Shape functions $\Psi_i(z)$ for a nodal polynomial expansion visualized in global bases, and **(c)** in local bases (standard element).

This standard element $\Omega_{st}$ can be mapped to any elemental domain $\Omega^e$ using the isoparametric transformation $\chi^e(\xi)$, which expresses the global coordinate $z$ in terms of the local coordinate $\xi$, depicted in Fig. 3b–c.

A class of nodal $p$-type expansions, which also have become known as *spectral elements*, are based on Legendre polynomials. The polynomials are defined in the standard domain $\Omega_{st}$ according to

$$L_m(\xi) = \frac{1}{2^m\, m!} \frac{d^m(\xi^2-1)^m}{d\xi^m} \quad , \tag{21}$$

where $m$ denotes the degree of the used polynomial. Based on the Legendre polynomials the *spectral elements* are given by

$$\psi_p^e(\xi) = \frac{(1-\xi^2)L_m^{'}(\xi)}{m(m+1)L_m(\xi_p)(\xi_p-\xi)} \quad , \tag{22}$$

where $L_m$ is the Legendre polynomial of degree $m$, $L_m^{'}$ denotes the differentiation with respect to the argument, and $\xi_p$ is the $p$-th Gauss-Lobatto-Legendre quadrature point defined by the corresponding root of $(1-\xi^2)\, L_m^{'}(\xi) = 0$.

The choice of these quadrature point plays an important role in the stability of the approximation. The spectral elements $\psi_p^e(\xi)$ are shown in the standard domain $\Omega^e$ in Fig. 3 for $m = 4$, [7].

Finally, considering the approximated solution in terms of the spectral elements $\psi_p^e(\xi)$, we can express the approximate solution $\tilde{f}(z,t)$ in terms of $\psi_p^e(\xi)$ according to

$$\tilde{f}(z,t) = \sum_{j=0}^{N_{dof}-1} \Psi_j(z)\,\alpha_j(t) = \sum_{e=1}^{N_{el}} \sum_{p=0}^{m} \psi_p^e(\xi)\,\alpha_p^e(t) \tag{23}$$

where $\psi_p^e(\xi) = \psi_p([\chi^e]^{-1}(z))$ contains the transformation from local bases to global bases in terms of the *parametric mapping* $\chi^e(\xi)$. The coefficients $\alpha_j(t)$ in this form have a physical interpretation in that they represent the solution of the partial differential equation (1) at the nodal points $x_j$. This fact is exploited for the derivation of a simple measurement gain matrix $\mathbf{H}_k$, i.e., it turns out that it is reasonable to put the sensor nodes onto the polynomial nodes, see Sect. 4.2.

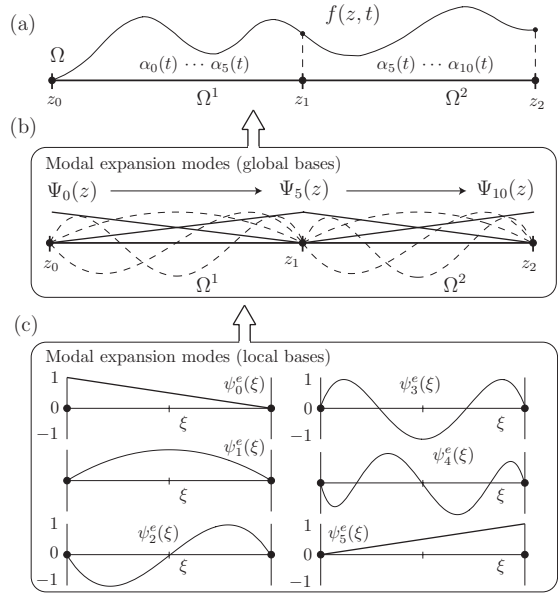


**Fig. 4** Approximation of the solution $f(z,t)$ by means of a modal polynomial expansion, e.g. Legendre polynomials for $m = 5$ refinement. **(a)** Elemental decomposition of the solution domain $\Omega$ into several subdomains $\Omega^e$. **(b)** Shape functions $\Psi_i(z)$ for a modal polynomial expansion visualized in global bases, and **(c)** in local bases (standard element).

Upon substituting the nodal expansion (23) into the weak formulation of the partial differential equation (13) the entries of the local mass matrices $M_{ij}^e$ and local diffusion matrices $D_{ij}^e$ can be derived as

$$M_{ij}^e = \int_{-1}^{1} \psi_i^e(\xi)\psi_j^e(\xi)d\xi \ ,$$
$$D_{ij}^e = \int_{-1}^{1} \frac{d\psi_i^e(\xi)}{d\xi}\frac{d\psi_j^e(\xi)}{d\xi}d\xi \ . \tag{24}$$

Considering the boundary conditions at the elemental nodes, e.g. $z_1$ and $z_2$ in Fig. 3, the local matrices $M_{ij}^e$ and $D_{ij}^e$ can be easily assembled to the global mass matrix $\mathbf{M}_G$ and global diffusion matrix $\mathbf{D}_G$. This is an automatic procedure known as *global assembly*.

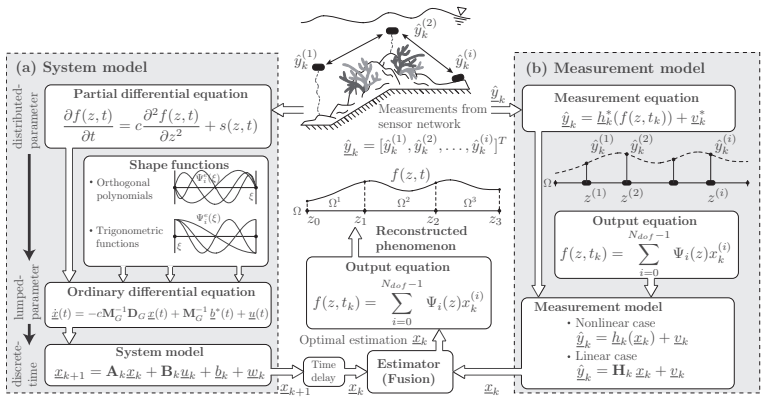


**Fig. 5** Overview and components of the procedure for model-based reconstruction of distributed phenomena. **(a)** System model: conversion of the distributed-parameter system into a lumped-parameter discrete-time system, **(b)** Measurement model: relating specific measurements $\underline{\hat{y}}_k$ to the underlying distributed phenomenon. The estimated state vector $\underline{x}_k$ from the system model and the measurement model is used to obtain optimal estimation result, and thus the reconstruction of the distributed phenomenon.

### 3.4 Modal Polynomial Expansions

For the construction of $p$-type expansions it is often favorable to select a set of orthogonal functions (polynomials), such as Legendre polynomials, Chebyshev polynomials or sine functions. The most commonly used orthogonal polynomials in computational fluid dynamics, which offer some advantages compare to the other polynomials, are based upon the Legendre polynomials. The $p$-type modal expansion modes in the standard element $\Omega_{st}$ are defined as

$$\psi_p^e(\xi) = \begin{cases} \frac{1-\xi}{2} & p = 0 \\ (1-\xi^2)L'_{p-1}(\xi) & 0 < p < m \\ \frac{1-\xi}{2} & p = m \end{cases} \ , \tag{25}$$

where the lowest expansion modes $\psi_0(\xi)$ and $\psi_p(\xi)$ are the same as in the linear finite element expansion. These modes are denoted as boundary modes since they are the

only modes which are nonzero at the ends of the interval. In Fig. 4 the $p$-type modal expansion based upon the Legendre polynomials is depicted for $m = 5$, [11].

Thus, the approximate solution $\tilde{f}(z,t)$ in terms of a modal polynomial expansion can be expressed in the same manner as the nodal polynomial expansion (23); the function $\psi_p^e(\xi)$ is just replaced by $p$-type modal expansion modes (25) and the coefficients $\alpha_j(t)$ denote the weighting coefficients for the individiual *modes*. The local mass matrices $M_{ij}^e$ and local diffusion matrices $D_{ij}^e$ can be derived similar to the nodal polynomial expansion (24). Considering the boundary conditions at the end of each element, e.g. $z_1$ in Fig. 4, the local matrices $M_{ij}^e$ and $D_{ij}^e$ can be easily assembled to the global mass matrix $\mathbf{M}_G$ and global diffusion matrix $\mathbf{D}_G$.

## 4 Temporal Discretization of ODE-System

In the previous section, we presented the spatial decomposition allowing the conversion of the partial differential equation into a set of ordinary differential equation, i.e., the conversion of the distributed-parameter system into a lumped-parameter system. In this section, we are now ready to specifiy the time evolution leading to the discrete-time system model (3) and the discrete-time measurement model (5).

### 4.1 System Model

To circumvent the restriction on the time step $\Delta t$, it is reasonable to integrate the set of ordinary differential equations (14) by means of *implicit* methods, such as the Crank-Nicolson discretization. Basically, this discretization method selects a time step $\Delta t$, evaluates the differential equation at time $t + \frac{1}{2}\Delta t$, and finally approximates the time derivative on the left-hand side of (14) with a centered finite difference and the rest of the terms with averages, leading to

$$\mathbf{M}_G \frac{\underline{x}_{k+1} - \underline{x}_k}{\Delta t} = \mathbf{M}_G \underline{u}_k - \frac{c}{2}\mathbf{D}_G \left[\underline{x}_{k+1} + \underline{x}_k\right] + \underline{b}_k^*$$

Rearranging, the Crank-Nicolson discretization of the differential equation produces a linear system of equations for the state vector $\underline{x}_{k+1}$ containing the unknown weighting factors $\alpha_i$ at the $k+1$ time step,

$$\left(\mathbf{M}_G + \frac{1}{2}c\Delta t\mathbf{D}_G\right)\underline{x}_{k+1} = \left(\mathbf{M}_G - \frac{1}{2}c\Delta t\mathbf{D}_G\right)\underline{x}_k$$

$$+\Delta t\mathbf{M}_G\underline{u}_k + \Delta t\underline{b}_k^* \ .$$

It is important to note that this linear system is *unconditionally* stable for any time step $\Delta t$. Using the following abbreviations

$$\mathbf{A}_k = \left(\mathbf{M}_G + \frac{1}{2}c\Delta t\mathbf{D}_G\right)^{-1}\left(\mathbf{M}_G - \frac{1}{2}c\Delta t\mathbf{D}_G\right),$$

$$\mathbf{B}_k = \Delta t \left( \mathbf{M}_G + \frac{1}{2} c \Delta t \mathbf{D}_G \right)^{-1} \mathbf{M}_G \ ,$$

$$\underline{b}_k = \Delta t \left( \mathbf{M}_G + \frac{1}{2} c \Delta t \mathbf{D}_G \right)^{-1} \underline{b}_k^* \ ,$$

and adding noise terms and modelling error terms the linear system can be stated in the well-known compact state space form

$$\underline{x}_{k+1} = \mathbf{A}_k \, \underline{x}_k + \mathbf{B}_k \, \underline{u}_k + \underline{b}_k + \underline{w}_k \ , \tag{26}$$

where the matrices $\mathbf{A}_k$ and $\mathbf{B}_k$ are determined using the global mass matrix $\mathbf{M}_G$ and the global diffusion matrix $\mathbf{D}_G$. The vector $\underline{b}_k$ containing the boundary conditions is determined using the matrices $\mathbf{M}_G$, $\mathbf{D}_G$, and the boundary vector $\underline{b}_k^*$. Fig. 5a visualizes the conversion of a distributed phenomenon characterized by means of a partial differential equation from the distributed-parameter form into a lumped-parameter form, and finally into a discrete-time finite-dimensional state space form.

The resulting physical model in finite-dimensional state space form (26) could be used for the simulation of the underlying distributed phenomenon by propagating the finite-dimensional state vector $\underline{x}_k$ over time. Then, the desired result $\tilde{f}(z,t)$ of the underlying distributed phenomenon could be directly derived by using the equation for the approximated solution (6).

However, for a model-based reconstruction method by means of a sensor network the aim is not just the simulation of the distributed phenomenon, rather the reconstruction of that phenomenon by means of discrete-time measurements from the sensor network. Unfortunately, for most applications the measurements have to be regarded as uncertain values containing the uncertainties of the actual sensor node. In order to take these uncertainties of both the measurements and the system model into account, it is common to use appropriate parameterized density functions for the description of the *estimated* state vector $\underline{x}_k$. This will be specified in more detail in Sect. 5. Before it is essential to derive a description mapping the specific measurements to the solution of the observed phenomenon; the so-called measurement model.

### 4.2 Measurement Model

For model-based reconstruction not only a system model of the distributed phenomenon is necessary but also a measurement model, which maps the specific measurements $\hat{\underline{y}}_k$ obtained from the sensor network to the solution $f(z,t)$ of the observed phenomenon. This section is devoted to the derivation of the discrete-time measurement model.

By means of the spatial decomposition, introduced in Sect. 3, it is possible to derive a relation between the individual measurements $\hat{\underline{y}}_k$ and the entire observed phenomenon. The sensor nodes, which are densely deployed inside the distributed phenomenon, are used to observe that phenomenon and to improve its estimated state $\underline{x}_k$. The measurement model consists of two parts: the measurement equation and the output equation.

The measurement equation relates the actual measurements $\hat{y}_k^{(i)}$ at location $z^{(i)}$ and at time $t_k$ to the distributed phenomenon $f(z, t_k)$, according to

$$\underline{\hat{y}}_k = \underline{h}_k^*(f(z, t_k)) + \underline{v}_k^* \ , \tag{27}$$

where the vector $\underline{v}_k^*$ contains the uncertainties arising from the actual sensor node. Even for simple measurement principles the mapping $\underline{h}_k^*(.)$ consists of non-linear functions. In such cases non-linear approaches for the estimation algorithm have to be applied.

The output equation, on the other hand, relates the punctiform measurements of the distributed phenomenon $f(z^{(i)}, t_k)$ directly to the finite-dimensional state vector $\underline{x}_k$, according to

$$f(z^{(i)}, t_k) = \sum_{j=0}^{N_{dof}-1} \Psi_j(z^{(i)}) x_k^{(j)} \ , \tag{28}$$

which is identical to the representation of the approximated solution $\tilde{f}(z, t)$ of the partial differential equation introduced in Sect. 3.1.

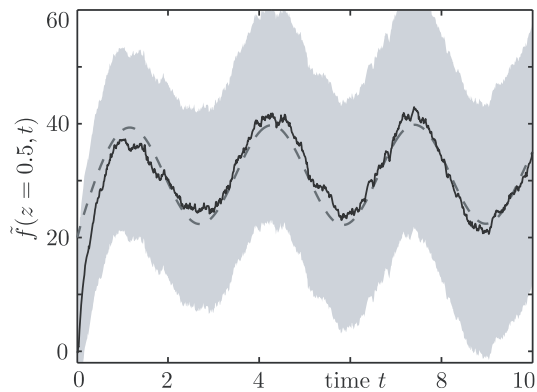


**Fig. 6 Prediction:** estimated solution $\tilde{f}(z, t)$ (black), $3\sigma$-Bounds (gray shaded), and analytic solution $f(z, t)$ (black dotted).

Substitution of the output equation (28) into the measurement equation (27) leads to the complete measurement model, which provides the mapping of the individual discrete-time measurements $\underline{\hat{y}}_k$ obtained from the sensor network to the finite-dimensional state vector $\underline{x}_k$ characterizing the state of the distributed phenomenon. For the nonlinear case the measurement model is given by

$$\underline{\hat{y}}_k = \underline{h}_k(\underline{x}_k) + \underline{v}_k \ ,$$

and for the linear case the measurement model is given by

$$\underline{\hat{y}}_k = \mathbf{H}_k \underline{x}_k + \underline{v}_k \ ,$$

where $\underline{v}_k$ are the measurement uncertainties arising from both the sensor node and the modeling errors. Fig. 5b shows the complete measurement model relating specific

measurements $\underline{\hat{y}}$ to the underlying distributed phenomenon in terms of the state vector $\underline{x}_k$.

In this article, for simplicity and brevity only the linear case is considered. That means, the measurement of the $i$-th sensor node at the location $z^{(i)}$ and at time step $k$, i.e., $t = t_k$, is related to the state vector $\underline{x}_k$ according to

$$\begin{aligned}\hat{y}_i(z^{(i)}, t = t_k) &= \sum_{j=0}^{N_{dof}-1} \Psi_j(z^{(i)})\, \alpha_j(t = t_k) \\ &= \underline{\Psi}^T(z^{(i)})\, \underline{x}_k.\end{aligned}$$

Assuming a sensor network consisting of $L$ sensor nodes, the measurement gain matrix $\mathbf{H}_k$ is set up by the shape function $\underline{\Psi}^T(z^{(i)})$ of order $N$, according to

$$\underline{\hat{y}}_k = \underbrace{\begin{pmatrix} \Psi_1(z^{(1)}) & \cdots & \Psi_N(z^{(1)}) \\ \vdots & \ddots & \vdots \\ \Psi_1(z^{(L)}) & \cdots & \Psi_N(z^{(L)}) \end{pmatrix}}_{\mathbf{H}_k} \underline{x}_k + \underline{v}_k \ , \tag{29}$$

where $\underline{v}_k$ are the measurement uncertainties. The number of rows $L$ of the matrix $\mathbf{H}_k$ depends on the number of used sensors, i.e., number of measurement points, and the number of columns $N$ depends on the desired number of modes.

However, in the case of nodal expansion and assuming that the sensors are located at the polynomial nodes, i.e., $z^{(i)} = z_i$, the weighting coefficients can be measured directly, i.e., $\alpha_j(t) = \hat{y}_j$. In other words, the diagonal entries of the measurement gain matrix $\mathbf{H}_k$ are either 1 or 0, depending on the location of the sensor nodes,

$$\underline{\hat{y}}_k = \underbrace{\begin{pmatrix} 1 & \cdots & 0 \\ \vdots & \ddots & \vdots \\ 0 & \cdots & 1 \end{pmatrix}}_{\mathbf{H}_k} \underline{x}_k + \underline{v}_k \ . \tag{30}$$

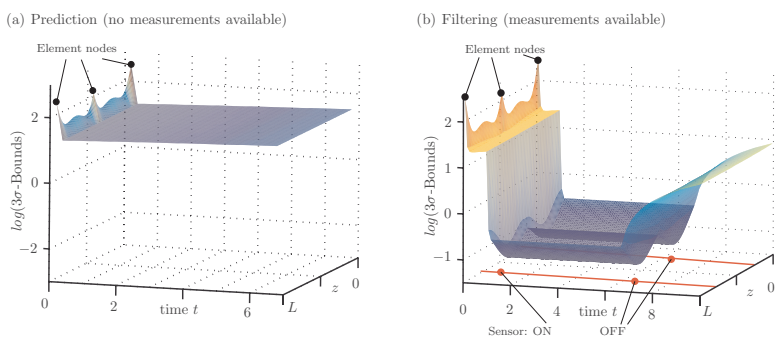


**Fig. 7** Logarithm of the $3\sigma$-Bounds as a measure for the uncertainty of the estimated solution $\tilde{f}(z,t)$. **(a)** Uncertainty for the prediction (no measurements available), **(b)** Uncertainty for filtering (measurements available). Due to the measurements the uncertainty can be decreased rapidly, even between the sensor nodes.

# 5 Centralized Estimation Approach

In this section, the prediction step and the filter step for a centralized estimation approach are derived. Due to the fact that both the system equation (26) and the measurement equation (5) are linear, it is sufficient to use the linear Kalman filter [10] [17] to obtain the best possible estimate for the system state characterizing the distributed phenomena.

## 5.1 Prediction Step

The purpose of the prediction step is to propagate the current state estimate $\underline{\hat{x}}_k^e$ through the system equation (26) to the next time step. Thus, the mean of the predicted state vector $\underline{\hat{x}}_{k+1}^p$ at time step $k+1$ is given by

$$\underline{\hat{x}}_{k+1}^p = \mathbf{A}_k \, \underline{\hat{x}}_k^e + \mathbf{B}_k \, \underline{\hat{u}}_k + \underline{\hat{b}}_k \quad .$$

Assuming that the input vector $\underline{u}_k$ and the state vector $\underline{x}_k$ are uncorrelated the covariance matrix is obviously given by

$$\mathbf{C}_{k+1}^p = \mathbf{A}_k \, \mathbf{C}_k^e \, \mathbf{A}_k^T + \mathbf{B}_k \, \mathbf{C}_k^u \mathbf{B}_k^T + \mathbf{C}_k^d \quad ,$$

where $\mathbf{C}_k^e$ is the covariance matrix of the state estimate $\underline{x}_k^e$, $\mathbf{C}_k^u$ is the covariance matrix of the input noise, and $\mathbf{C}_k^d$ is the covariance matrix of subsumed endogenous uncertainties, e.g. modeling errors.

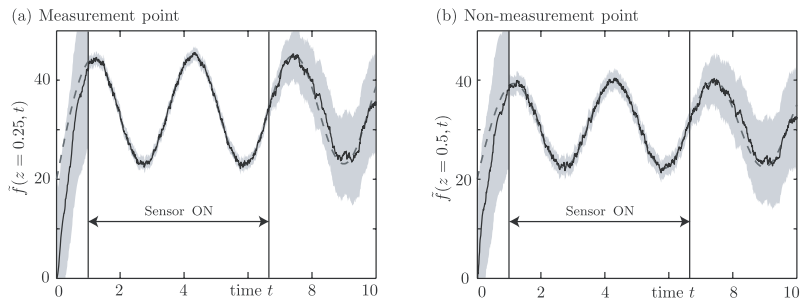


**Fig. 8 Filtering:** estimated solution $\tilde{f}(z,t)$ (black), $3\sigma$-Bounds (gray shaded), and analytic solution $f(z,t)$ (black dotted) at **(a)** measurement point and **(b)** non-measurement point.

The simulation results of the prediction of the distributed phenomenon (estimation without using measurements) is shown in Fig. 6 and in Fig. 7a. The details of the simulation are explained in more detail in Sect. 6. Here, it can be easily recognized that the certainty of the estimated solution $\tilde{f}(z,t)$ cannot be increased, i.e., only the propagation of the estimated state vector $\underline{x}_k$ seems not to be sufficient.

### 5.2 Filter Step

For the purpose of reducing the estimation uncertainty, measurements are used that are related to the state via the measurement equation (5). Given the predicted state $\underline{\hat{x}}_k^p$ with covariance $\mathbf{C}_k^p$ and a vector observation $\underline{\hat{y}}_k$ with covariance $\mathbf{C}_k^v$, the estimated state vector $\underline{\hat{x}}_k^e$ is derived by

$$\begin{aligned}\underline{\hat{x}}_k^e =& \underline{\hat{x}}_k^p + \mathbf{C}_k^p \mathbf{H}_k^T \left(\mathbf{C}_k^v + \mathbf{H}_k \mathbf{C}_k^p \mathbf{H}_k^T\right)^{-1} \\ & \cdot \left(\underline{\hat{y}}_k - \mathbf{H}_k \underline{\hat{x}}_k^p\right)\end{aligned}$$

In the uncorrelated case the covariance matrix of the estimate is given by

$$\mathbf{C}_k^e = \mathbf{C}_k^p - \mathbf{C}_k^p \mathbf{H}_k^T \left(\mathbf{C}_k^v + \mathbf{H}_k \mathbf{C}_k^p \mathbf{H}_k^T\right)^{-1} \mathbf{H}_k \mathbf{C}_k^p \ .$$

The simulation results of the filtering (estimation using measurements) is shown in Fig. 7b and in Fig. 8. The details of the simulation are explained in more detail in Sect. 6. Here, it can be easily recognized that the certainty of the estimated solution $\tilde{f}(z,t)$ can be significantly increased by using additional information in terms of measurements from the sensor network.

## 6 Simulation Results

In this section we demonstrate the performance of the proposed estimation method by means of simulations. The goal is the reconstruction of the temperature distribution in a

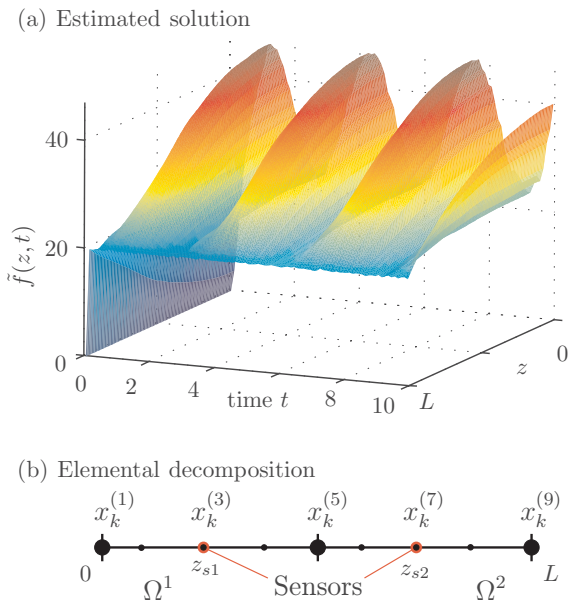


**Fig. 9 (a)** Estimated solution $\tilde{f}(z,t)$. **(b)** Elemental decomposition into two elements $\Omega_1$ and $\Omega_2$ with a polynomial expansion of order $m = 5$ and location of sensor nodes.

heat rod using both a physical model and measurements obtained by a sensor network. It is important to note that a novelty of our approach is to consider the uncertainties arising from noisy measurements and occuring in the physical model (state vector and input vector).

The evolution of the temperature is modelled by the well-known one-dimensional heat equation (1) of a bar with the length $L = 1\,\mathrm{m}$. The noisy input function is given by $s(z,t) = 30\,\sin(2\,t) + 30 + \Delta u_k$, where $\Delta u_k$ denotes the input uncertainties. Applying a nodal expansion (23) for the approximated solution $\tilde{f}(z,t) = \underline{\Psi}^T(z)\,\underline{\alpha}(t)$, the partial differential equation (1) can be spatially and temporally decomposed leading to the *finite*-dimensional state space form (26). The state vector $\underline{x}_k$ can be derived by temporal discretization of the weighting factors $\underline{\alpha}(t)$ of the approximated solution, as shown in Sect. 4. Here, we assume a nodal expansion based on a Legendre polynomial of the order $m = 5$. The spatial decomposition of the heat rod into two elements $\Omega_1$ and $\Omega_2$ is visualized in Fig. 9b.

Furthermore, it is assumed that for simplicity the sensor network consists of two sensor nodes located at $z_{s1} = 0.25$ and $z_{s2} = 0.75$, shown in Fig. 9b. In the case of a nodal expansion the general relation between the measurement vector $\hat{\underline{y}}_k$ and the state vector $\underline{x}_k$ described by (29) can be simplified to (30). For this simulation example that means the state variables $x_k^{(3)}$ and $x_k^{(7)}$ can be measured directly, as it is visualized in Fig. 9b.

The estimated solution $\tilde{f}(z,t)$ is visualized in Fig. 9a. The logarithm of the $3\sigma$-bound of the estimated solution $\tilde{f}(z,t)$, which is a measure for its uncertainty, is depicted in Fig. 7a for prediction which means the propagation of the estimated solution $\tilde{f}(z,t)$ without using measurements from the sensor network and in Fig. 7b for the filtering which means measurements from the sensor network are exploited to improve the estimated solution $\tilde{f}(z,t)$. It is obvious that the measurements are used for rapidly decreasing the uncertainty. Thanks to the model-based approach they can be decreased even *between* the sensor nodes; the remaining uncertainty merely arises from the model uncertainties.

The estimation results for both a measurement point and a non-measurement point are visualized in Fig. 8. Again, it can easily be seen that the solution $\tilde{f}(z,t)$ is estimated even at non-measurement points with an appropriate certainty. Furthermore, it is clear that by means of the measurements the estimated solution $\tilde{f}(z,t)$ can be significantly improved.

## 7 Conclusions

This chapter introduced the methodology for deriving system models and measurement models for the reconstruction of distributed phenomena characterized by means of linear partial differential equations. Thanks to the inhomogeneous approximation capabilities and the systematic manner of this approach, the estimation of nonlinear phenomena even with complex geometries is possible. The novelty of this chapter is the model-based reconstruction of distributed phenomena under the consideration of uncertainties both occuring in the physical model and arising from noisy measurements.

It is believed that applying such methods in sensor network applications for the reconstruction provides novel prospects to optimal sensor node placement, optimal measurement time sequences, and improvement of the used physical model. The performance of the proposed model-based approach for the reconstruction of distributed pheonmena was demonstrated by means of simulation results for the one-dimensional partial differential equation.

For the one-dimensional linear partial differential equation, the decomposition may seem unnecessarily involved. However, the same principles can easily be applied to the decomposition in multiple dimensions and even for nonlinear partial differential equation. This is left for future research work.

As it was mentioned in the introduction, the estimation results can be exploited for several additional tasks, such as optimal sensor placement, model improvement, and system identification. Especially the problem of system identification would be essential for sensor networks performing self-organization in a completely unknown sourrounding. By using such methods for the identification of an appropriate physical model of the sourrounding it would be possible for the sensor nodes to identify, observe, and reconstruct unknown distributed phenomena. This is also part of future research work.

Furthermore, especially for large sensor networks it is essential to find a decentralized reconstruction approach. It is believed that the decomposition method introduced in this chapter is well-suited for such an estimation approach. The application of decentralized data fusion methods such as introduced in [8] [21] for a decentralized reconstruction approach is left for future research work.

## Acknowledgements

This work was partially supported by the German Research Foundation (DFG) within the Research Training Group GRK 1194 “Self-organizing Sensor-Actuator-Networks”.

## References

1. Anderson, B. D. O. and Moore, J. B. (1979). *Optimal Filtering*. Prentice-Hall.
2. Baker, A. J. (1983). *Finite Element Computational Fluid Mechanics*. Taylor and Francis.
3. Brunn, D. and Hanebeck, U. D. (2005). A model-based framework for optimal measurements in machine tool calibration. In *IEEE International Conference on Robotics and Automation (ICRA 2005)*, Barcelona, Spanien.
4. Culler, D. E. and Mulder, H. (2004). Smart sensors to network the world. In *Scientific American*, volume 6.
5. Fagherazzi, S., Furbish, D. J., Rasetarinera, P., and Hussaini, M. Y. (2004). Application of the discontinuous spectral Galerkin method to groundwater flow. In *Advances in Water Resources*, volume 27, pp. 129–140.
6. Faulds, A. L. and King, B. B. (2000). Sensor location in feedback control of partial differential equation systems. In *Proceedings of the 2000 IEEE International Conference on Control Applications (CCA 2000)*, pp. 536–541, Anchorage, AK.
7. Fournier, A., Bunge, H.-P., Hollerbach, R., and Vilotte, J.-P. (2004). Application of the spectral-element method to the axisymmetric Navier-Stokes equation. In *Geophysical Journal International*, number 156, pp. 682–700.

8. Hanebeck, U. D. and Briechle, K. (2001). New results for stochastic prediction and filtering with unknown correlations. In *Proceedings of the IEEE Conference on Multisensor Fusion and Integration for Intelligent Systems (MFI 2001)*, pp. 147–152, Baden-Baden, Germany.
9. Hanebeck, U. D., Briechle, K., and Rauh, A. (2003). Progressive Bayes: a new framework for nonlinear state estimation. In *Proceedings of SPIE, AeroSense Symposium*, pp. 256–267, Orlando, Florida.
10. Kalman, R. E. (1960). A new approach to linear filtering and prediction problems. In *Transactions of the ASME Journal of Basic Engineering*, issue 82, pp. 34–45.
11. Karniadakis, G. E. and Sherwin, S. (2005). *Spectral/HP Element Methods for Computational Fluid Dynamics*. Oxford University Press.
12. Komatitsch, D., Ritsema, J., and Tromp, J. (2002). The spectral-element method, Beowulf computing, and global seismology. In *Science*, volume 298, pp. 1737–1742.
13. Komatitsch, D., Vilotte, J.-P., Vai, R., Castillo-Covarrubias, J. M., and Sanchez-Sesma, F. J. (1999). The spectral element method for elastic wave equations – application to 2-D and 3-D seismic problems. In *International Journal for Numerical Methods in Engineering*, volume 45, pp. 1139–1164.
14. Kumar, T., Zhao, F., and Shepherd, D. (2002). Collaborative signal and information processing in microsensor networks. In *IEEE Signal Processing Magazine*, volume 19, pp. 13–14.
15. Levin, J. G., Iskandarani, M., and Haidvogel, D. B. (2000). A nonconforming spectral element ocean model. In *International Journal for Numerical Methods in Fluids*, volume 34, pp. 495–525.
16. Ortmaier, T., Groeger, M., Boehm, D. H., Falk, V., and Hirzinger, G. (2005). Motion estimation in beating heart surgery. In *IEEE Transactions on Biomedical Engineering*, volume 52, issue 10, pp.1729–1740.
17. Papoulis, A. (1991). *Probability, Random Variables and Stochastic Processes*. McGraw-Hill.
18. Rao, B., Durrant-Whyte, H., and Sheen, J. (1993). A fully decentralized multisensor system for tracking and surveillance. In *International Journal of Robotics Research*, volume 12, pp. 20–44.
19. Roberts, K. and Hanebeck, U. D. (2005). Prediction and reconstruction of distributed dynamic phenomena characterized by linear partial differential equations. In *The 8th International Conference on Information Fusion (Fusion 2005)*, Philadelphia, USA.
20. Sawo, F., Brunn, D., and Hanebeck, U. D. (2006a). Parameterized joint densities with gaussian mixture marginals and their potential use in nonlinear robust estimation. In *IEEE International Conference on Control Applications (CCA 2006)*, Munich, Germany.
21. Sawo, F., Roberts, K., and Hanebeck, U. D. (2006b). Bayesian estimation of distributed phenomena using discretized representations of partial differential equations. In *Proceedings of the 3rd International Conference on Informatics in Control, Automation and Robotics (ICINCO 2006)*, pp. 16–23, Setubal, Portugal.
22. Thuraisingham, B. (2004). Secure sensor information management and mining. In *IEEE Signal Processing Magazine*, volume 5, pp. 14–19.